

The broad-band *XMM–Newton* and *INTEGRAL* spectra of bright type 1 Seyfert galaxies

F. Panessa^{1,2}, L. Bassani³, A. De Rosa¹, A.J. Bird⁴, A.J. Dean⁴, M. Fiacchi¹, A. Malizia³, M. Molina⁴, P. Ubertini¹, R. Walter^{5,6}

¹ IASF-Roma/INAF, Via Fosso del Cavaliere 100, I-00133 Rome, Italy

² Instituto de Física de Cantabria (CSIC-UC), Avda. de los Castros, 39005 Santander, Spain

³ IASF-Bologna/INAF, Via P. Gobetti 101, I-40129 Bologna, Italy

⁴ School of Physics and Astronomy, University of Southampton, Southampton, SO17 1BJ, UK

⁵ INTEGRAL Science Data Centre, CH-1290 Versoix, Switzerland

⁶ Geneva Observatory, University of Geneva, Chemin des Maillettes 51, 1290 Sauverny, Switzerland

Preprint online version: October 24, 2018

ABSTRACT

Aims. The 0.5–150 keV broad-band spectra of a sample of nine bright type 1 Seyfert galaxies are analyzed here. These sources have been discovered/detected by INTEGRAL and subsequently observed with XMM–Newton for the first time with high sensitivity below 10 keV. The sample, although small, is representative of the population of type 1 AGN which are now being observed above 20 keV.

Methods. The intrinsic continuum has been modeled using three different parameterizations: a power-law model, an exponential cut-off power-law and an exponential cut-off power-law with a Compton reflection component. In each model the presence of intrinsic absorption, a soft component and emission line reprocessing features has also been tested.

Results. A simple power-law model is a statistically good description of most of the spectra presented here; an FeK line, fully and/or partial covering absorption and a soft spectral component are detected in the majority of the sample sources. The average photon index ($\langle \Gamma \rangle = 1.7 \pm 0.2$) is consistent, within errors, with the canonical spectral slope often observed in AGN although the photon index distribution peaks in our case at flat Γ (~ 1.5) values. For four sources, we find a significantly improved fit when the power-law is exponentially cut-off at an energy which is constrained to be below ~ 150 keV. The Compton reflection parameter could be estimated in only two objects of the sample and in both cases is found to be $R > 1$.

Key words. galaxies: Seyfert – X-rays: galaxies

1. Introduction

It is widely accepted that the hard X-ray emission from Active Galactic Nuclei (AGN) is primarily produced via unsaturated inverse Compton scattering of UV–soft X-ray photons from the accretion disk by a corona of hot, probably thermal, electrons (e.g., Haardt & Maraschi 1991, Zdziarski et al. 2000, Kawaguchi et al. 2001). The emitted X-ray photon spectrum is best described by a power law and an exponential cut-off at high energies. A reprocessing component is typically superimposed onto the cut-off power-law continuum, emerging at energies > 10 keV and is interpreted as Compton reflection of the power-law photons off thick matter that can be the accretion disk itself and/or the torus envisaged in unified models. This component is typically accompanied by an iron K fluorescence line.

In recent years, the excellent performances of the *XMM–Newton* and *Chandra* satellites have provided very good quality X-ray spectra of Seyfert galaxies, allowing a proper determination of the spectral parameters of the primary continuum and the superimposed complex reprocessing features (see, e.g., Nandra et al. 2007, McKernan et al. 2007, Piconcelli et al. 2005, Pounds & Reeves 2002). However, *BeppoSAX* spectra of Seyfert galaxies have shown that broad-band observations are necessary to better constrain the slope of the primary continuum and the

value of the e-folding energy which has so far only been properly measured in a few sources (Guainazzi et al. 1999, Perola et al. 2002). In addition, the determination of the Compton reflection component R (the solid angle in units of 2π subtended by the reflecting material) is inadequate when observations are restricted to less than 10 keV.

The advent of the *INTEGRAL* and *Swift* satellites is significantly improving our knowledge of AGN spectra above 20 keV. Their all-sky hard X-ray surveys are increasing the statistics and demography of nearby AGN (Markwardt et al. 2005, Krivonos et al. 2005, Bassani et al. 2006, Beckmann et al. 2006, Sazonov et al. 2007) and are allowing a characterization of their hard X-ray properties (Beckmann et al. 2006, Ajello et al. 2008, Winter et al. 2008, Molina et al. 2006, Malizia et al. 2007, Tueller et al. 2008, De Rosa et al. 2008).

In particular, the unique capabilities of the IBIS (Ubertini et al. 2003) instrument on board *INTEGRAL* allow the detection of sources above 20 keV at the mCrab level with an angular resolution of $12'$ and a typical point source localization accuracy of $2\text{--}3'$. During its first few years of life, *INTEGRAL* has surveyed a large portion of the sky, detecting many Galactic/extra-galactic objects and discovering new/unidentified sources (Bird et al. 2006, 2007, Bassani et al. 2006), many of which now identified as AGN. Here we present the *XMM–Newton* and *INTEGRAL* broad-band spectral analysis of a sample of 9 sources associated with active galaxies: eight of them have been observed for the first time below 10 keV with the high sensitivity allowed

Table 1. Sample of *INTEGRAL* AGN.

| Name (1) | RA (2) | Dec (3) | Class (4) | z (5) | N_H (6) | $F_{20-40keV}^{\dagger}$ (7) | Ref. (8) |
|-----------------|-----------|------------|--------------|----------|--------------|---------------------------------|-------------|
| LEDA 168563 | 73.021 | 49.546 | S1 | 0.0290 | 0.54 | 3.6±0.5 | 1 |
| IGR J07597-3842 | 119.923 | -38.719 | S1.2 | 0.0400 | 0.60 | 2.2±0.2 | 2 |
| ESO 209-12 | 120.507 | -49.753 | S1.5 | 0.0405 | 0.238 | 0.9±0.2 | 1 |
| Fairall 1146 | 129.620 | -36.013 | S1.5 | 0.0316 | 0.40 | 1.2±0.2 | 1 |
| 4U1344-60 | 206.883 | -60.610 | S1.5 | 0.0129 | 1.07 | 4.3±0.2 | 3 |
| IGR J16482-3036 | 252.050 | -30.590 | S1 | 0.0313 | 0.17 | 1.7±0.2 | 3 |
| IGR J16558-5203 | 254.010 | -52.062 | S1.2 | 0.0540 | 0.304 | 1.8±0.1 | 2 |
| IGR J17418-1212 | 265.474 | -12.215 | S1 | 0.0372 | 0.217 | 1.4±0.2 | 4 |
| IGR J18027-1455 | 270.685 | -14.916 | S1 | 0.0350 | 0.496 | 2.5±0.1 | 5 |

Note: (1): Galaxy name. (2)-(3): Equatorial J2000 coordinates. (4): Optical classification. (5) Redshift. (6): Galactic absorption in units of 10^{22} cm^{-2} . (7): Time average flux expressed in units of mCrab (20-40 keV: 10 mCrab = 7.57×10^{-11} $\text{erg cm}^{-2} \text{s}^{-1}$), Bird et al. 2007. (8): References: 1. NED position and classification; 2. Masetti et al. 2006a; 3. Masetti et al. 2006b; 4. Torres et al. 2004; 5. Masetti et al. 2004.

by *XMM-Newton*, despite being all very bright X-ray sources (a few mCrab level or $2\text{-}10 \times 10^{-11}$ $\text{erg cm}^{-2} \text{s}^{-1}$ in the 20-100 keV band). All of them have been optically classified as Seyfert galaxies of type 1-1.5 (Masetti et al. 2004, 2006a, 2006b).

The wide energy range covered by jointly fitting the *XMM-Newton* and *INTEGRAL* data up to 150 keV offers an opportunity to characterize the spectral continuum and estimate, whenever possible, the exponential cut-off energy and the reflection component. Ideally, one would prefer to have X-ray and soft gamma-ray data taken simultaneously, but this is now possible only through pointing observations like those obtained by the *Suzaku* observatory. *INTEGRAL*, however, has the advantage of having detected a number of new AGN for which *XMM-Newton* observations are available. Even with the limitation of non simultaneous measurements, analysis of broad-band data of a large sample of objects provides clues on the overall high energy properties of type 1 Seyfert galaxies.

The paper is organized in the following manner: Section 2 describes the sample and the *INTEGRAL* data used; Section 3 describes the *XMM-Newton* data reduction procedure; Section 4 illustrates the broad-band *XMM-Newton* and *INTEGRAL* spectral fitting procedures in general and for each individual source; Section 5 is devoted to the discussion of the different spectral components found and their possible correlations. Finally, in Section 6 we report our conclusions. Throughout this paper we assume a flat Λ CDM cosmology with $(\Omega_M, \Omega_\Lambda) = (0.3, 0.7)$ and a Hubble constant of $70 \text{ km s}^{-1} \text{ Mpc}^{-1}$ (Bennett et al. 2003).

2. The Seyfert sample and the *INTEGRAL* data

The sample analyzed in the present work is extracted from the Bassani et al. (2006) survey, updated to include a number of optical classifications obtained afterwards (see Bassani, Malizia and Stephen 2006). The sample includes Seyfert 1-1.5 galaxies with a 20-100 keV flux less than 5 mCrab, for which *XMM-Newton* data were available at the time of writing. From the sample we have excluded sources already studied over a similar broad energy band, i.e., eight type 1-1.5 Seyfert galaxies listed in Bassani et al. (2006) survey are below the chosen threshold flux: four (NGC 4593, NGC 6814, MKN 6 and MCG-6-30-15) have already been studied (Perola et al. 2002, Molina et al. 2006, Malizia et al. 2003a, Guainazzi et al. 1999, respectively) and the remaining four (2E 1853.7+1534, ESO 323-G077, ESO 511-G030 and IGR J16119-6036) had no *XMM-Newton* data available or public at the time this analysis was conducted.

All nine objects in the sample have been detected in X-rays before, but with the exception of 4U 1344-60, the available data were of poorer quality or limited to soft energy ranges (i.e., below 3 keV) than those presented here. None of the objects in the present sample had spectral information available in the soft gamma-ray range prior to this study, except 4U 1344-60 (Beckmann et al. 2006). Overall we can conclude that the sample used in this work is representative of the population of type 1 AGN detected by *INTEGRAL* above 20 keV and consists of objects poorly studied so far.

The *INTEGRAL* data presented here consist of several pointings performed by the low-energy instrument IBIS/ISGRI (*INTEGRAL* Soft Gamma-Ray; Lebrun et al. 2003) between revolution 12 and 429, i.e. the period from launch (October 2002) to the end of April 2006. The IBIS/ISGRI images for each available pointing were generated in various energy bands using the ISDC off-line scientific analysis software OSA version 5.1 (see e.g., Goldwurm et al. (2003) for the ISGRI data analysis within OSA). Count rates at the position of the source were extracted from individual images in order to provide light curves in various energy bands; from these light curves average fluxes were then estimated and combined to obtain the source spectrum (see Bird et al. 2006, 2007, for details).

In Table 1 we report the list of objects analyzed and the relevant information for each of them such as, the coordinates for epoch J2000, the optical classification, the redshift, the Galactic column density, the 20-40 keV *INTEGRAL* flux as reported in Bird et al. (2007) and the optical identification references.

For each AGN, we checked in the *XMM-Newton* field of view (typically a radius of $15'$) for the presence of sources which might contribute to the high energy flux. Except for IGR J07597-3842, no bright sources were found. At $\sim 4'$ from the nuclear position of IGR J07597-3842, a bright point-like source is clearly detected in the image. Its *XMM-Newton* spectrum is dominated by a strong soft component, while the 2-10 keV flux is only 6×10^{-14} $\text{erg cm}^{-2} \text{s}^{-1}$; therefore we do not expect this source to contribute significantly to the *INTEGRAL* flux.

Finally, we remind the reader that while *XMM-Newton* are snap-shot observations, *INTEGRAL* provides an average spectrum over many ks exposures spanning a few years period.

3. The *XMM-Newton* data reduction

All objects in the sample have been observed between March and August 2006. The data have been processed starting from the

Table 2. *XMM-Newton* Data Observation Details

| Name | Obs. Date | Exposure pn | Filter | Counts/bin |
|-----------------|------------|----------------|--------|------------|
| (1) | (2) | (3) | (4) | (5) |
| LEDA 168563 | 2007-02-26 | 9314 | medium | 100 |
| IGR J07597-3842 | 2006-04-08 | 13260 | thin | 100 |
| ESO 209-12 | 2006-03-25 | 5789 | thin | 20 |
| FRL 1146 | 2006-04-15 | 3941 | thin | 20 |
| FRL 1146 | 2006-12-12 | 7087 | thin | 35 |
| 4U1344-60 | 2001-08-25 | 25000 | medium | 35 |
| IGR J16482-3036 | 2006-03-01 | 6784/6296 | medium | 20 |
| IGR J16558-5203 | 2006-03-01 | 6227 | medium | 20 |
| IGR J17418-1212 | 2006-04-04 | 12109 | thin | 50 |
| IGR J18027-1455 | 2006-03-25 | 16645 | thin | 50 |

Notes: (1): Galaxy name. (2): Observation date. (3): pn observation exposures except for IGR J16482-3036 for which MOS1/MOS2 observation exposure is reported. (4): pn filters. (5): Number of counts per bin used to rebin the spectral channels.

odf files with the *XMM-Newton* SAS software (version 7.0.0). Given its higher sensitivity, we use the time average EPIC/pn spectrum for the analysis of each object, except for IGR J16482-3036 for which only EPIC/MOS data are available. X-ray events corresponding to patterns 0-12 and 0-4 were selected from the MOS and pn, respectively. We used the most updated calibration files available at the time of the reduction for each source data. Source light curves and spectra were extracted from circular regions of typically 50'' centered on the source, while background products were obtained from off-set regions close to the source. Exposures have been filtered for periods of high background and the effective exposures are reported in Table 2 as well as the observation date, the pn filter and the number of counts per bin used to rebin the spectral channels. Spectra were binned according to the luminosity of each source. The ancillary and detector response matrices were generated using the *XMM-Newton* SAS *arfgen* and *rmfgen* tasks.

4. The *XMM-Newton* and *INTEGRAL* spectral analysis

The *XMM-Newton* and *INTEGRAL* data were fitted together and analyzed using XSPEC v.12.4.0. Since the *XMM-Newton* and *INTEGRAL* observations are not simultaneous, a cross-calibration constant C has been introduced in our best-fit models. This has been done to take into account possible cross-calibration mismatches between the two instruments or variability in the sources. The constant was left free to vary and, for each fit, its value is reported in the relevant Table. Galactic absorption is implicitly included in all spectral models; abundances are those of Anders & Grevesse (1989). The errors, lower and upper limits quoted correspond to 90% confidence range for one interesting parameter (i.e. $\Delta\chi^2 = 2.71$; Avni 1976).

The broad-band 0.5-150 keV *XMM-Newton* and *INTEGRAL* spectrum of each source has been initially fitted with a power-law model absorbed by intrinsic cold absorption, plus a soft X-ray component and a narrow Gaussian emission (Fe) line. A simple parameterization has been employed to model the soft component found to be present in six of our sources: either a black body or a MEKAL thermal plasma model with temperature kT provided a good description of the data, except for LEDA 168563, where a soft power-law model (Γ_{soft}) was instead preferred. All detected FeK α emission lines were found to be consistent with a narrow Gaussian profile, so that the line width was fixed to $\sigma = 10$ eV. In a few sources, the quality of

the fit improves significantly with the introduction of additional spectral components such as a partial covering absorption (*pcfabs* model in XSPEC) in 4U 1344-60 and IGR J16558-5203. An extra Gaussian emission line is instead required in IGR J17418-1212 and IGR J18027-1455; finally an absorption edge was required in the case of FRL 1146 (AO4).

In Table 3 we show the best-fit parameters together with the model fluxes in the 2-10 keV and 20-100 keV bands. Although the best-fit solutions are obtained by including the additional spectral components described above, the values of their parameters are not included in Table 3 but are discussed in detail, for each source, in the next subsection.

To check for the presence of a high energy cut-off, we replaced the simple power-law in the best-fit model used in Table 3, with one having an exponential cut-off (*cutoffpl* model in XSPEC) and report in Table 4 the results provided by this change on the main fit parameters. Finally, to also take into account the possible presence of a reflection component, we replaced the exponentially cut-off power-law with the *pexrav* model in XSPEC. The reflection component is described by two fundamental parameters: $R = \Omega/2\pi$, which is the fraction of a neutral, plane parallel slab illuminated by the power-law photons, and i or the slab inclination angle with respect to the line of sight. Since all parameters turned out to be identical to those obtained with $\cos i$ left free to vary, we choose to freeze $\cos i$ to 0.45. In Table 5 we report the values obtained for the *pexrav* main spectral parameters.

In the next subsection, we briefly describe, for each individual source, the best-fit models and the values of the additional spectral components which, for the sake of clarity, have not been reported in the Tables. Note also that the values of the absorption, FeK line and soft component parameters do not vary significantly between the power-law, cut-off power-law and *pexrav* model fits, and therefore they have not been included in Table 4 and Table 5. In Fig. 1 and Fig. 2, the unfolded spectrum and the baseline parameterization, together with the contributions to the model of the various additive components are shown for each object (best-fit model).

4.1. Notes on individual sources

LEDA 168563. The combined *XMM-Newton* and *INTEGRAL* spectrum is well fitted by a hard power-law model plus a soft power-law component with $\Gamma = 3.8^{+0.2}_{-0.2}$. A narrow Gaussian component at ~ 6.4 keV is statistically significant at $\sim 95\%$

Table 3. Best fit spectral parameters using an absorbed power-law, a soft thermal component and a Gaussian narrow line.

| Name (1) | $N_{\text{H,int}}$ (2) | Γ (3) | E_{α} (4) | EW_{α} (5) | C (6) | kT/Γ_{soft} (7) | F_{2-10} (8) | F_{20-100} (9) | χ^2/dof (10) |
|------------------------------|---------------------------|------------------------|------------------------|----------------------|---------------------|----------------------------------|-------------------|---------------------|-----------------------------|
| LEDA 168563 | - | $1.68^{+0.05}_{-0.05}$ | $6.44^{+0.09}_{-0.11}$ | <52 | $0.6^{+0.2}_{-0.2}$ | $3.8^{+0.2}_{-0.2}$ | 1.46 | 5.6 | 507/488 |
| IGR J07597-3842 | - | $1.57^{+0.01}_{-0.02}$ | $6.44^{+0.04}_{-0.04}$ | 48^{+39}_{-13} | $0.8^{+0.1}_{-0.1}$ | $0.09^{+0.01}_{-0.01}$ | 1.56 | 3.6 | 352/339 |
| ESO 209-12 | - | $1.73^{+0.02}_{-0.03}$ | $6.39^{+0.04}_{-0.05}$ | 163^{+57}_{-62} | $1.2^{+0.3}_{-0.2}$ | $0.05^{+0.01}_{-0.01}$ | 0.83 | 1.9 | 500/508 |
| FRL 1146(AO3) | $0.36^{+0.05}_{-0.05}$ | $1.84^{+0.05}_{-0.05}$ | $6.39^{+0.07}_{-0.07}$ | <146 | $1.1^{+0.3}_{-0.3}$ | $0.15^{+0.02}_{-0.01}$ | 1.15 | 2.0 | 418/421 |
| FRL 1146(AO4) [†] | $0.28^{+0.04}_{-0.04}$ | $1.69^{+0.04}_{-0.08}$ | $6.37^{+0.03}_{-0.03}$ | 111^{+37}_{-20} | $0.7^{+0.2}_{-0.2}$ | $0.16^{+0.01}_{-0.01}$ | 1.21 | 2.0 | 424/438 |
| 4U1344-60 [†] | $0.98^{+0.14}_{-0.17}$ | $2.04^{+0.08}_{-0.09}$ | $6.41^{+0.04}_{-0.04}$ | 51^{+28}_{-19} | $0.9^{+0.1}_{-0.1}$ | - | 3.58 | 6.6 | 706/638 |
| IGR J16482-3036 | $0.09^{+0.01}_{-0.01}$ | $1.59^{+0.02}_{-0.03}$ | $6.46^{+0.06}_{-0.06}$ | 96^{+32}_{-72} | $0.5^{+0.1}_{-0.1}$ | - | 1.97 | 1.9 | 607/563 |
| IGR J16558-5203 [†] | - | $2.25^{+0.03}_{-0.03}$ | $6.48^{+0.05}_{-0.06}$ | 61^{+50}_{-34} | $2.7^{+0.5}_{-0.5}$ | - | 1.05 | 2.8 | 540/592 |
| IGR J17418-1212 [†] | $0.13^{+0.01}_{-0.01}$ | $1.98^{+0.01}_{-0.02}$ | $6.28^{+0.04}_{-0.05}$ | 51^{+37}_{-29} | $1.5^{+0.3}_{-0.3}$ | - | 1.29 | 2.1 | 651/606 |
| IGR J18027-1455 [†] | $0.41^{+0.05}_{-0.05}$ | $1.61^{+0.04}_{-0.04}$ | $6.39^{+0.05}_{-0.03}$ | 134^{+33}_{-34} | $2.9^{+0.3}_{-0.3}$ | $0.19^{+0.08}_{-0.07}$ | 0.61 | 4.6 | 363/316 |

Note: (1): Galaxy name. (2): Intrinsic fully-covering column density in units of 10^{22} cm^{-2} . (3): Power-law photon index. (4): Energy of the FeK line, in keV. (5): Equivalent width of the FeK line, in eV. (6): Value of the *XMM-Newton/INTEGRAL* cross-calibration constant. (7): Temperature of the thermal component (kT in keV) or photon index of the soft power-law component (Γ_{soft}) in the case of LEDA 168563. (8-9): Model fluxes in the 2-10 keV and 20-100 keV bands in units of $10^{-11} \text{ erg cm}^{-2} \text{ s}^{-1}$. (10): Chi-squared and degrees of freedom. †: Sources with extra spectral components (see Section 4).

Table 4. Best fit spectral parameters using an exponential cut-off power-law model.

| Name (1) | Γ (2) | $E_{\text{cut-off}}$ (3) | C (4) | χ^2/dof (5) |
|-----------------|------------------------|-----------------------------|---------------------|----------------------------|
| LEDA 168563 | $1.59^{+0.08}_{-0.10}$ | 73^{+152}_{-36} | $0.9^{+0.2}_{-0.3}$ | 500/487 |
| IGR J07597-3842 | $1.51^{+0.03}_{-0.04}$ | 64^{+40}_{-20} | $1.4^{+0.3}_{-0.3}$ | 327/338 |
| ESO 209-12 | $1.73^{+0.02}_{-0.03}$ | > 60 | $1.5^{+0.3}_{-0.4}$ | 497/507 |
| FRL 1146(AO3) | $1.81^{+0.04}_{-0.04}$ | > 45 | $1.3^{+0.7}_{-0.5}$ | 417/420 |
| FRL 1146(AO4) | $1.61^{+0.09}_{-0.08}$ | > 29 | $1.1^{+0.6}_{-0.4}$ | 422/437 |
| 4U1344-60 | $1.75^{+0.08}_{-0.14}$ | > 78 | $0.8^{+0.2}_{-0.1}$ | 698/636 |
| IGR J16482-3036 | $1.53^{+0.04}_{-0.04}$ | 65^{+52}_{-24} | $0.7^{+0.2}_{-0.2}$ | 590/562 |
| IGR J16558-5203 | $2.25^{+0.01}_{-0.01}$ | > 134 | $2.9^{+0.7}_{-0.3}$ | 540/591 |
| IGR J17418-1212 | $1.97^{+0.02}_{-0.02}$ | > 170 | $1.6^{+0.3}_{-0.3}$ | 651/605 |
| IGR J18027-1455 | $1.53^{+0.05}_{-0.05}$ | 108^{+75}_{-32} | $3.6^{+0.6}_{-0.5}$ | 341/315 |

Note: (1): Galaxy name. (2): Power-law photon index. (3): Energy of the exponential cut-off in keV. (4): Value of the *XMM-Newton/INTEGRAL* cross-calibration constant. (5): Chi-squared and degrees of freedom.

Table 5. Best fit spectral parameters using a pexrav model.

| Name (1) | Γ (2) | $E_{\text{cut-off}}$ (3) | R (4) | C (5) | χ^2/dof (6) |
|-----------------|------------------------|-----------------------------|---------------------|---------------------|----------------------------|
| LEDA 168563 | $1.67^{+0.14}_{-0.17}$ | > 41 | < 1.69 | $0.7^{+0.9}_{-0.3}$ | 499/486 |
| IGR J07597-3842 | $1.48^{+0.05}_{-0.03}$ | 52^{+32}_{-7} | < 0.59 | $1.5^{+0.1}_{-0.2}$ | 328/338 |
| ESO 209-12 | $1.71^{+0.02}_{-0.03}$ | > 62 | < 0.77 | $1.5^{+0.5}_{-0.5}$ | 497/506 |
| FRL 1146(AO3) | $2.13^{+0.09}_{-0.09}$ | > 48 | < 2.00 | $0.7^{+0.3}_{-0.2}$ | 407/419 |
| FRL 1146(AO4) | $1.68^{+0.08}_{-0.06}$ | > 30 | < 2.63 | $0.9^{+0.8}_{-0.4}$ | 421/436 |
| 4U1344-60 | $1.78^{+0.14}_{-0.15}$ | > 94 | < 2.83 | $0.7^{+0.2}_{-0.3}$ | 698/635 |
| IGR J16482-3036 | $1.62^{+0.07}_{-0.07}$ | 87^{+97}_{-22} | $1.6^{+1.5}_{-1.1}$ | $0.4^{+0.2}_{-0.1}$ | 591/561 |
| IGR J16558-5203 | $2.30^{+0.04}_{-0.05}$ | - | < 9.63 | $1.1^{+1.6}_{-0.6}$ | 537/590 |
| IGR J17418-1212 | $2.07^{+0.05}_{-0.05}$ | - | $2.0^{+1.1}_{-0.9}$ | $0.9^{+0.2}_{-0.2}$ | 637/605 |
| IGR J18027-1455 | $1.48^{+0.01}_{-0.01}$ | > 400 | < 0.35 | $3.8^{+0.7}_{-0.7}$ | 338/314 |

Note: (1): Galaxy name. (2): Power-law photon index. (3): Energy of the exponential cut-off in keV. (4): Reflection parameter. (5): Value of the *XMM-Newton/INTEGRAL* cross-calibration constant. (6): Chi-squared and degrees of freedom.

confidence level (equivalent width < 52 eV). A cut-off power-law model is required by the data with a probability $P > 99\%$, allowing a good constraint on the cut-off energy of $E_{\text{cut-off}} = 73^{+152}_{-36}$ keV, while when using the *pexrav* model, only an upper limit for the reflection parameter is obtained;

the marginal evidence for a weak iron line also suggests a low reflection component. Indeed, if C is fixed to 1, the cut-off energy lowers slightly, while the upper limit on the reflection component becomes 0.6 instead of 1.7, more in line with the measured iron line equivalent width. The *Swift*/XRT 2-10

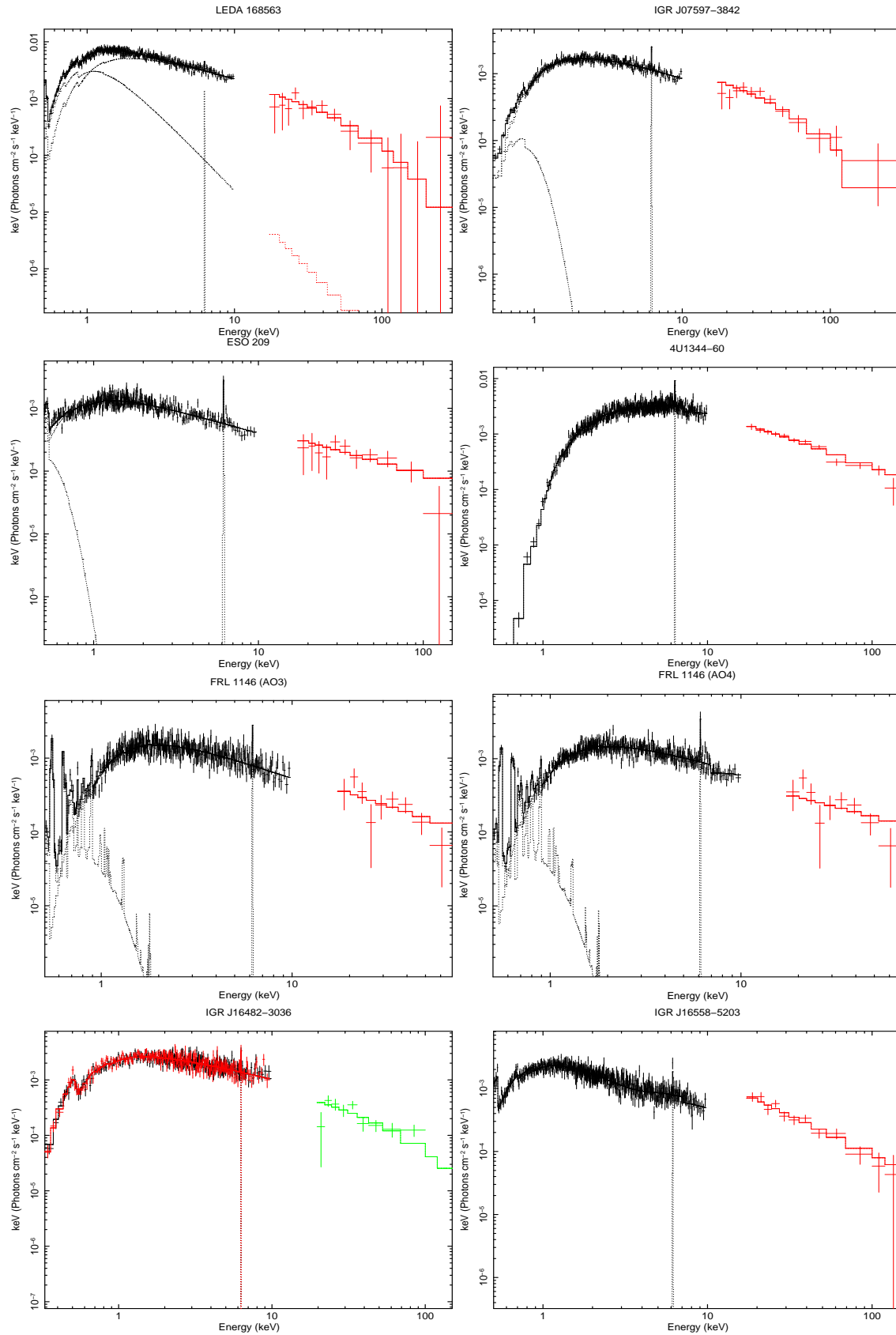


Fig. 1. The *XMM-Newton* and *INTEGRAL* best-fit spectra. Power-law model: ESO 209-12, FRL 1146 (AO3, AO4) and IGR J16558-5203. Exponential cut-off power-law: LEDA 168563, IGR J07597-3842 and IGR J16482-3036.

keV flux of this source (Malizia et al. 2007) is in good agreement with the one measured in this work and, together with

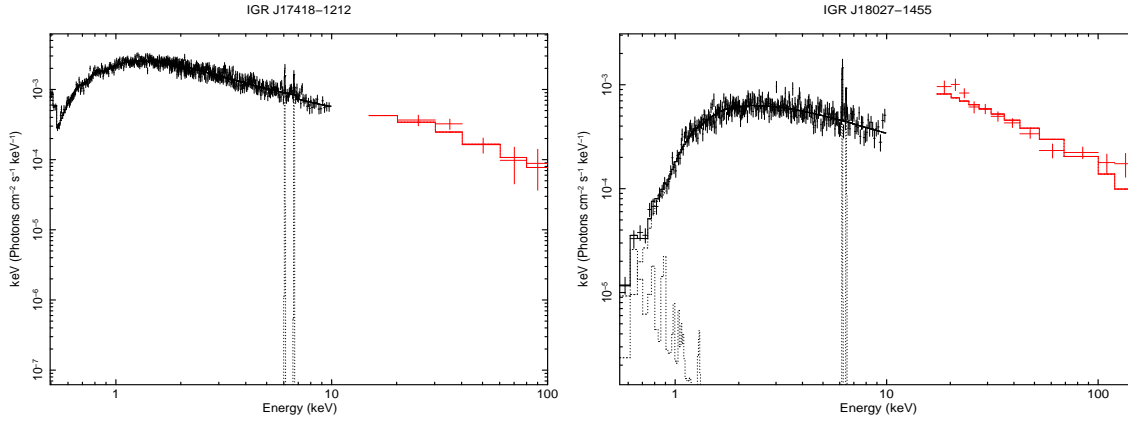


Fig. 2. Continued - The *XMM-Newton* and *INTEGRAL* best-fit spectra. Exponential cut-off power-law: IGR J18027-1455. *Pexrav* model: IGR J17418-1212.

the values of C , indicates that this source is not strongly variable.

IGR J07597-3842. The combined EPIC pn and *INTEGRAL* spectrum of this source is quite flat ($\Gamma \sim 1.6$) when fitted with the model of Table 3. The soft component is well represented by a black body with $kT = 0.09 \pm 0.01$ keV. The addition of a line at 6.4 keV significantly improves the fit ($P > 99.99\%$). Also a cut-off power-law model is highly required by the data ($P > 99.99\%$) with a cut-off energy at 64^{+40}_{-20} keV. Employing a *pexrav* model instead of the cut-off power-law does not improve the fit and, only yields an upper limit to the reflection parameter ($R < 0.59$). If the cross-calibration constant is fixed to 1, the cut-off energy moves around 80 keV and the reflection becomes ~ 0.4 . The 2-10 keV flux measured by *Swift*/XRT (Malizia et al. 2007) is a factor of ~ 1.6 higher than the one we measure with *XMM-Newton*, indicating possible variability in the source.

ESO 209-12. A simple power-law model for the combined *INTEGRAL* and *XMM-Newton* spectra, plus a black body component at $kT = 0.05$ keV and an iron line at ~ 6.4 keV provides a good fit of the spectrum. The addition of a second Gaussian component at $6.63^{+0.07}_{-0.08}$ keV improves the fit with a probability $P > 98\%$. A fit obtained using a cut-off power-law is equally good but only gives a lower limit to the high energy cut-off (> 60 keV). Similarly, a *pexrav* model provides an acceptable fit to the overall source spectrum but no constraint on the cut-off energy, and a reflection parameter ($R < 0.77$) are obtained. Fixing $C = 1$, the fit results in a flatter spectrum, a similar lower limit to the reflection, but a better constraint on the cut-off energy.

FRL 1146. This source has been observed twice by *XMM-Newton*. The first observation was performed on April 15th 2006 and the second on December 12th of the same year. No flux variability was observed between the two observations and both spectra could be fitted with a similar spectral model, i.e., a power-law model with intrinsic absorption ($N_{H,int} = 3.6 \pm 0.5$ for the first observation and $2.8 \pm 0.4 \times 10^{21}$ cm $^{-2}$, for the second one), plus a MEKAL component for the soft emission ($kT \sim 0.15$ keV in both measurements). The presence of an iron line at ~ 6.4 keV is marginally significant in the first observation ($P \sim 95\%$) but highly significant in the second one ($P > 99.99\%$). An edge at $6.93^{+0.13}_{-0.13}$ keV with an optical depth of $0.26^{+0.11}_{-0.11}$ is also significantly ($P \sim 99.95\%$) detected in the second observation only. The main difference between the two measurements is the

slope of the power-law, which is steeper in the first exposure. The cut-off energy is not properly constrained when a cut-off power-law model is used, nor is the reflection component in the case of the *pexrav* model. For both observations C is compatible with 1 within uncertainties so fixing it to this value is acceptable, but should be regarded with caution given the observed spectral variability: in this case the fit with *pexrav* provides a cut-off energy at around 50 keV and an upper limit for R of 0.8 for the second measurement.

4U 1344-60. The *XMM-Newton* data of this source have already been analyzed by Piconcelli et al. (2006), while the combined *XMM-Newton* and *INTEGRAL* spectrum has been previously discussed by Beckmann et al. (2006) who obtained a good representation of the broad-band data with an absorbed power-law plus a Gaussian component. Here, in addition to the power-law model, we used a fully-covering absorber ($N_H = 9.8 \times 10^{21}$ cm $^{-2}$) plus two layers of absorbing material partially covering the source ($N_H^{pc1} = 4.7^{+1.4}_{-1.2} \times 10^{22}$ cm $^{-2}$, $C_{vrF^{pc1}} = 0.61^{+0.06}_{-0.05}$ and $N_H^{pc2} = 43^{+16}_{-10} \times 10^{22}$ cm $^{-2}$, $C_{vrF^{pc2}} = 0.50^{+0.06}_{-0.07}$). The values obtained for the fully-covering absorption and for the first layer of partially covering material are consistent with those reported in Piconcelli et al. (2006). However, our fit improves significantly (with a probability $> 99.99\%$) with the addition of a second absorbing layer of material partially covering the AGN. A cut-off power-law model marginally improves the quality of the fit with a probability of $\sim 97\%$; however, only a lower limit is found for the high energy cut-off (> 78 keV) and an upper limit to the reflection parameter ($R < 2.8$) if a *pexrav* model is used. If C is fixed to 1 (which is barely allowed by the data) in the *pexrav* model, the cut-off energy is constrained to be around 140 keV and the reflection component to be < 0.1 which is not consistent with the value of the iron line equivalent width; clearly in this case a fit with a free C is to be preferred.

IGR J16482-3036. The pn odF files of this source could not be reprocessed forcing us to use in this case MOS1 and MOS2 data together with the *INTEGRAL* data. The broad-band spectrum is well fitted by a simple power-law model absorbed by very mild intrinsic absorption. A narrow Gaussian component at $6.48^{+0.08}_{-0.09}$ keV is marginally detected ($P \sim 97\%$); an additional narrow Gaussian component at ~ 8 keV is significant with a probability of $P \sim 96\%$. Possible models which could explain the presence of an emission feature at such energies are

discussed in Gallo et al. (2005), who detected a similar feature. A cut-off power-law model significantly ($P > 99.99\%$) improves the quality of the fit, allowing a constraint to be put on the high energy cut-off at ~ 65 keV. Using the *pexrav* model, the fit does not improve but provides a constrained value for the reflection component of ~ 1.6 . The *Swift*/XRT data of this source show a spectral slope of $1.71^{+0.11}_{-0.12}$ plus intrinsic absorption (Malizia et al. 2007), in perfect agreement with the *XMM-Newton* data when fitted with the same model. The *XMM-Newton* 2-10 keV flux is slightly higher (1.97×10^{-11} erg cm $^{-2}$ s $^{-1}$) than the *XRT* one of 1.13×10^{-11} erg cm $^{-2}$ s $^{-1}$. In addition, the cross-calibration constant is much higher than 1, suggesting that IGR J16482-3036 is a variable AGN.

IGR J16558-5203. The spectrum of this source is well described by a steep power-law absorbed by a partially covering medium, significantly required with a probability $> 99.99\%$. The column density found for the partial absorber is $30^{+11}_{-8} \times 10^{22}$ cm $^{-2}$, and the covering fraction is $0.56^{+0.06}_{-0.05}$. The presence of an iron line at 6.4 keV is significant at only 94% confidence level. When introduced in the fit, the cut-off energy is constrained to be above 130 keV, but the cross-calibration constant is quite high both in the simple and cut-off power-law models. When the broad-band spectrum is instead fitted with a *pexrav* model, C is close to 1 but the reflection fraction is poorly constrained below 9.6. If C is fixed to 1 in the same model, the cut-off energy remains unconstrained and R becomes $6.6^{+3.1}_{-2.9}$. This source has also been observed by *Swift*/XRT and its power-law slope is $1.85^{+0.06}_{-0.04}$, slightly flatter than that observed with the pn data alone ($\Gamma = 2.08 \pm 0.01$). The *XRT* 2-10 keV flux is 1.77×10^{-11} erg cm $^{-2}$ s $^{-1}$ (Malizia et al. 2007), slightly higher than the *XMM-Newton* one.

IGR J17418-1212. The broad-band continuum of this source is well represented by the *pexrav* model; fixing the cut-off energy to a high value (which is compatible with $E_{\text{cut-off}} \geq 170$ keV as indicated by the cut-off power-law fit), the reflection parameter is constrained to be $R = 2.0^{+1.1}_{-0.9}$ and the cross-calibration constant is found to be around 1. A first narrow Gaussian component at $6.28^{+0.04}_{-0.04}$ keV is significant with a 99.99% probability, while a second component at $6.74^{+0.04}_{-0.06}$ keV (equivalent widths of 63^{+49}_{-21} eV) is also strongly required by the data with a similar probability ($\sim 99.96\%$).

IGR J18027-1455. The extrapolation of the *XMM-Newton* spectrum to the 20–100 keV band falls short with respect to the *INTEGRAL* detected flux; this is reflected in the relatively high values of the cross-calibration constant (~ 3) found in our fits. The continuum is well described by a cut-off power-law model which allows the cut-off energy to be constrained to around 100 keV. Only a lower limit is obtained for the reflection fraction ($R < 0.35$) and a high value of the cross-calibration constant is found ($C \sim 4$). If the cross-calibration constant is fixed to 1, the value of R becomes $3.2^{+2.2}_{-0.3}$, suggesting a strong reflection component, which is more compatible (but still too high) with the equivalent width (134^{+33}_{-34} eV) of the iron line at 6.4 keV. An extra narrow Gaussian component is detected at $6.67^{+0.06}_{-0.08}$ keV ($P \sim 99.80\%$) with an equivalent width of 61^{+37}_{-28} eV.

5. Discussion

The broad-band spectra analyzed here are all well represented, to a first approximation, by a power-law model accompanied in

many cases by extra features: a fully and/or partial covering absorption, a soft component, one or two narrow Gaussian components and an absorption edge. If the power-law model is replaced by a cut-off power-law model, the fit significantly improves in the case of LEDA 168563, IGR J07597-3842, IGR J16482-3036 and IGR J18027-1455. The use of the *pexrav* model allows us to constrain the reflection component only in two objects, i.e., IGR J16482-3036 and IGR J17418-1212, but only in the latter case is this model significantly required by the data. The cross-calibration constant has been left free to vary in all our fits and it ranges from 0.4 to 3.8, with a mean value of 1.28 in the case of the power-law model, 1.57 for the exponential cut-off power-law model and 1.22 when employing the *pexrav* model. If C is fixed to 1, when this is compatible with the measured values, better constraints on the cut-off energy and reflection are obtained and, in most cases, these are compatible with the results reported in Tables 4 and 5. However, due to the non-simultaneity of the *XMM-Newton* and *INTEGRAL* observations, spectral and/or flux variability could play an important role in the determination of the spectral parameters (as in the case of Fairall 1146 where the spectral slope varied significantly between two different *XMM-Newton* observations). In the following discussion, we choose to adopt those fits where C is left free to vary. Even in this case, some caution is still worthwhile, but we hope that the sampling of several objects dilutes any remaining effects of combining non-simultaneous data sets and provides some indications on the average high energy properties of type 1 AGN. In the following, we discuss in detail the main results of our analysis.

5.1. The intrinsic absorption and the soft X-ray spectrum

In five objects of the sample, mild neutral absorption in excess of the Galactic value is highly required to improve the quality of the fit; the observed column densities range from 0.09 to 9.8×10^{21} cm $^{-2}$. In the case of two sources, the absorption is complex as it partially covers one source (IGR J16558-5203), or, as in the case of 4U1344-60, is formed by two layers of material partially obscuring the central source. In the case of intermediate Seyfert galaxies, such as 4U1344-60, this is in agreement with the Unified Model predictions, since at intermediate angles of the line of sight only the outer part of the obscuring torus is intercepted by the observer (e.g., see Maiolino 2001 and references therein). In the case of IGR J16558-5203, the high value of its absorption could be instead ascribed to an intercepting cloud, a concept discussed, for instance, in Lamer et al. (2003) and also envisaged in the clumpy torus model proposed by Elitzur & Shlosman (2006). In several type 1 Seyfert galaxies, complex absorption has also been found in the form of a warm absorber (Gondoin et al. 2003, Schurch & Warwick 2003; Feldmeier et al. 1999), often used to describe the soft X-ray spectrum of type 1 AGN. Since it is beyond the scope of this work to assess the ionization state and temporal variability of this absorber, we have chosen to describe the soft part of the spectrum with a simple model adequate to ensure a proper parameterization of the X-ray/gamma-ray spectrum. In fact, a soft power-law with $\Gamma = 3.8$ (for LEDA 168563), a black body with temperature 0.09 and 0.05 keV (for IGR J07597-3842 and ESO 209-12, respectively) and a MEKAL model with kT of 0.15 and 0.19 keV (for FRL 1146 and IGR J18027-1455 respectively) provide quite good fit to the soft energy continuum of our sources. Clearly a more detailed analysis of the *XMM-Newton* high-resolution data is needed to assess the nature of the soft component present in some of our sources and we defer this study to a future work.

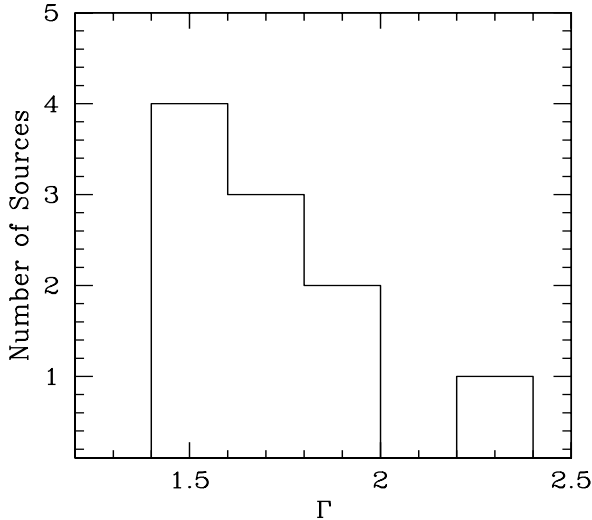


Fig. 3. Photon index distribution (data from Table 4). A binning of 0.2 in photon index has been used.

5.2. The intrinsic primary continuum and the high energy cut-off

In Fig. 3 we show the photon index distribution obtained from data in Table 4, where a cut-off power-law model is used. The mean Γ is 1.73 with a standard deviation of 0.24. This value is consistent, within errors, with the 2-10 keV mean slope found for other sample of AGN (i.e., $\langle \Gamma \rangle \sim 1.8-2$, Reeves & Turner 2000, Piconcelli et al. 2005, Dadina 2008). Four sources (LEDA 168563, IGR J07597-3842, IGRJ16482-3036 and IGRJ18027-1455) in our sample have very flat spectra, i.e., $\Gamma \sim 1.5-1.6$, providing the low Γ peak seen in Fig. 3. Our photon index distribution is similar to the one reported for a sample of nearby Seyfert 1-1.5 galaxies by Cappi et al. (2006) who found an even flatter weighted mean value for Γ (1.56 ± 0.04 compared to our 1.68 ± 0.02). Interestingly, flat photon indices have been invoked to account for the X-ray background spectral shape in synthesis models recently proposed (Gilli et al. 2007). There are several examples in the literature of type 1 sources with flat spectra (Mkn 841, Petrucci et al. 2007; PG 1416-129, Porquet et al. 2007; NGC 4051, Ponti et al. 2006; NGC 3516, Turner et al. 2005; NGC 3227, Gondoin et al. 2003; 1H 0419-577, Pounds et al. 2004); all of these sources are characterized by puzzling spectral and temporal behaviors. In general, the rather flat spectra of type 1 AGN can be ascribed to either the presence of a warm and/or complex absorber, or alternatively to a reflection bump as all of these components conspire to flatten the primary continuum. Another possible explanation for the detection of many flat spectrum sources could be the hard X-ray selection of our sample, i.e. AGN with a flat Γ and a significant reflection component (when present) are more easily detected at energies > 10 keV than objects with a steep continuum and no reflection. However, the average photon index found in hard X-rays surveys is $\Gamma \sim 2.1$ (see Beckmann et al. 2006, Deluit & Courvoisier 2003, Zdziarski et al. 1995) and indeed, if we fit the *INTEGRAL* data alone with a simple power-law, the average photon index turns out to be $\Gamma = 2.08 \pm 0.18$. Furthermore, objects with a flat primary continuum are not characterized by a particularly high reflection component (in fact R tends to be low in these objects). Further 2-10 keV data possibly on a complete sample of hard

X-ray selected AGN may help understanding if these 4 AGN are peculiar and rare objects or instead belong to a typical and more abundant than previously thought population.

The broad-band spectral analysis allowed us to constrain the high energy cut-off in four out of nine AGN in the sample and for all of them the cut-off energy is found to be below 150 keV. This is at odds with previous results which located the cut-off energy, on average, at ~ 200 keV for the type 1 Seyfert galaxies observed with *BeppoSAX* (Perola et al. 2002, Malizia et al. 2003b, Dadina 2008). Gondek et al. (1996), who analyzed the average 1-500 keV spectrum of type 1 AGN observed with *EXOSAT*, *Ginga*, *HEAO-1* and *CGRO OSSE*, found a cut-off energy > 500 keV; similarly a study by Zdziarski et al. (1995) of broad-band *Ginga* and *CGRO OSSE* spectra of a large sample of Seyferts provided $E_{cut-off} > 250$ keV. Moreover, only 6 of the 36 AGN detected by *INTEGRAL* analyzed by Beckmann et al. (2006) and Sazonov et al. (2004) require a cut-off at energies below 200 keV. On the other hand, there are spurious examples in the literature of type 1 Seyferts with low values of the high energy cut-off (e.g., Molina et al. 2006, Perola et al. 2002). Also the analysis of the average *BeppoSAX* PDS spectra by Deluit & Courvoisier (2003) shows that the lower limit obtained for type 1 Seyfert galaxies is fully consistent with our results ($E_{cut-off} > 63$ keV). This is also consistent with recent results by Ajello et al. (2008) who found a mean cut-off energy at ~ 100 keV in Seyfert 1 galaxies observed by *Swift/BAT*. A positive correlation between the cut-off energy versus the photon index was previously found using *BeppoSAX* data, first by Piro (1999), then by Petrucci et al. (2001) and finally confirmed by Perola et al. (2002). In Fig. 4 (left panel) we plot the cut-off energy (keV) versus the photon index Γ (data taken from Table 4). Given the poor statistical quality of our data, we cannot draw any conclusion on the correlation between these two parameters. However, no evidence of a correlation is found with the present data (censored data are not included in the analysis), although the four sources in which the cut-off energy has been constrained are those showing the flattest photon indices. We point out that the known interdependence of the parameters in the *pexrav* model (i.e., the cut-off energy is a variable in the fit which is strongly dependent on Γ and R) has to be taken into account when these correlations are discussed.

5.3. The reflection component and the Fe lines

A correlation between the reflection parameter R and the photon index has been claimed by Zdziarski et al. (1999) from the study of a large number of *Ginga* observations of Seyfert galaxies and Galactic black holes. However, the validity of this correlation is under debate, since R and Γ are strongly correlated in the fitting procedure (Vaughan & Edelson 2001) and subsequent works did not confirm the presence of a relation between these two parameters (Petrucci et al. 2001, Perola et al. 2002). Recently, Mattson, Weaver & Reynolds (2007) have shown that the strong correlation found between R and Γ in their sample of type 1 and type 1.2 Seyfert galaxies observed with *RXTE*, is likely to be an artefact of modeling degeneracy. The reflection parameter in our sample analysis is constrained only in IGR J16482-3036 and IGR J17418-1212. Therefore, the poor statistics and the large number of upper limits prevent us from drawing strong conclusions on this point. The R versus Γ (data taken from Table 5) plot is shown in Fig. 4, right panel: stronger reflection is indeed measured in steeper spectrum sources, but when upper limits are considered this effect is not so obvious in our data.

IGR J16482-3036, IGR J17418-1212 and possibly IGR J16558-5203 show a reflection component $R > 1$.

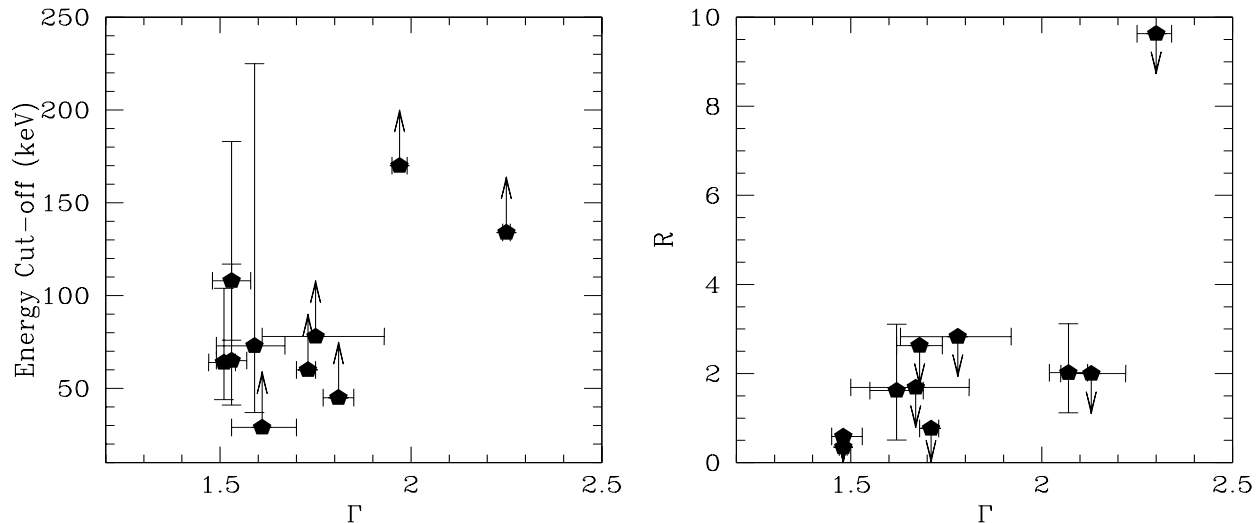


Fig. 4. Left panel: Energy cut-off (keV) versus Γ . Right panel: Reflection component R versus Γ .

These high values of R have been found in previous studies using *ASCA* and *BeppoSAX* data (Cappi et al. 1996, Dadina 2008) and, more recently, with the *Suzaku* satellite (Miniutti et al. 2007, Comastri et al. 2007). Such strong reflection might be present when more primary X-ray radiation is emitted toward the reflector than toward the observer as is possible in the case of strongly variable nuclear emission or when there is a time delay between the underlying continuum and the reflected component, caused by a large distance between the reflecting material and the primary source (Malzac & Petrucci 2002). Another explanation might be a peculiar geometry (Malzac et al. 2001; Malzac 2001) or general relativistic light bending effects (Fabian et al 2004; Miniutti & Fabian 2004; Fabian et al 2005). Recently, Gandhi et al. (2007) have shown that, in the synthesis models of the X-ray background spectrum, a significant fraction of this type of source is needed when light bending effects are taken into account.

Under the hypothesis that the line emission is entirely associated with optically thick material, the equivalent width of the Fe line is expected to correlate linearly with the value of R obtained for an arbitrarily fixed inclination angle. To a first approximation, an equivalent width of 140 eV is predicted if $R = 1$ for a cold, face-on disk and an incident power-law with $\Gamma \sim 2$ (George & Fabian 1991). In the case of IGR J16482-3036, the equivalent width (104^{+25}_{-82} eV), measured using the model in Table 5) is consistent with the observed reflection fraction; while in the case of IGR J17418-1212 it is very modest (41^{+26}_{-26} eV). Some scatter in the equivalent width could be introduced by a variance in the iron abundance which we do not take into account in our analysis. On the other hand, this discrepancy can be explained in terms of a possible anisotropy of the source of seed photons which might modify the resulting spectrum (Petrucci et al. 2001, Merloni et al. 2006).

For a given R , the equivalent width may also differ according to the value of Γ . The simulations of George & Fabian (1991) showed that the equivalent width of the iron line should decrease as the spectrum softens, given the presence of fewer photons with energies above the iron photoionization threshold. Mattson, Weaver & Reynolds (2007) further indicated that the correlation between these two parameters is not so simple. In fact, they ob-

served a positive trend which reverses at $\Gamma \sim 2$, i.e., the equivalent width versus Γ plot shows a correlation for $\Gamma < 2$ and an anticorrelation for $\Gamma > 2$. Interestingly, the two sources with a constrained value of R reflect this behavior: IGR J16482-3036, for which the R value is in agreement with the equivalent width of the line, has a $\Gamma = 1.62 \pm 0.07$, while IGR J17418-1212, in which a low equivalent width of the line is found, has $\Gamma = 2.07 \pm 0.05$. Broad-band simultaneous observations, such as those performed by *Suzaku*, are highly recommended in order to confirm the presence of a strong reflection component in these objects.

6. Conclusions

The IBIS instrument on board *INTEGRAL* has allowed the detection of new bright Seyfert galaxies. Here, we have presented the broad-band spectral analysis of nine type 1 AGN, eight of them never observed before below 10 keV with the high sensitivity of *XMM-Newton*. The simultaneous fitting of the EPIC/pn (or MOS) *XMM-Newton* and IBIS *INTEGRAL* data allowed a description of the continuum in terms of an absorbed power-law, plus a thermal soft component and an FeK emission line. In addition to this simple description of the continuum, we have found several additional components, such as partial covering absorption, Gaussian components and/or absorption edges. We also checked for the presence of an exponential high energy cut-off and a Compton reflection component. Bearing in mind the limitations of our broad-band analysis, mainly due to the non-simultaneity of the *XMM-Newton* and *INTEGRAL* observations, we summarize our findings as follows:

- Intrinsic fully-covering absorption has been found in five sources of the sample. Partial covering absorption is required in 4U 1344-60 and IGR J16558-5203. The presence of Compton thin clouds and/or of the outer part of the torus along the line of sight to the observer (as predicted in Unified Models) might explain the measured column densities as well as the complexity of the absorber. A soft component at $E < 2$ keV is present in more than half of our sources.
- A power-law model provides a good approximation of the primary continuum of the AGN presented here and in the

- cases of LEDA 168563, IGR J07597-3842, IGR J16482-3036 and IGR J18027-1455, a high energy exponential cut-off is significantly required by the data. The introduction of a reflection component is statistically significant only for IGR J17418-1212.
- When we consider the best-fit model for each source, the mean photon index found is $\langle \Gamma \rangle = 1.73 \pm 0.24$, consistent with the mean values commonly found in AGN. However, the photon index distribution has a peak at $\Gamma \sim 1.5$ and a tail towards steeper indices.
 - When constrained, the cut-off energy is located below 150 keV and no evidence for a correlation between spectral slope and the high energy cut-off is found in our data, at odds with results in the literature (Piro 1999, Petrucci et al. 2001, Perola et al. 2002). However, the limited statistics prevent us from drawing firm conclusions on this point.
 - The reflection parameter R has been constrained in only two sources, namely IGR J16482-3036 and IGR J17418-1212; in both of them the reflection fraction is found to be high, i.e. $R > 1$. According to current theoretical models, the equivalent width of the Fe line should correlate linearly with the value of R . This correspondence is observed in IGR J16482-3036, but not in the case of IGR J17418-1212. Variance in the iron abundance and/or possible anisotropy of the source of seed photons could be responsible for the observed mismatch, as well as spectral and flux variability of the sources.
- Acknowledgements.* We thank the anonymous referee for constructive and valuable comments which improved our manuscript. The results reported here are based on observations obtained with ESA science missions *XMM-Newton* and *INTEGRAL*. The team acknowledges support by ASI-INAF I/023/05/0 grants. F.P. acknowledges support by a "Juan de la Cierva" fellowship and the Spanish Ministry of Education and Science, under project ESP2006-13608.
- ## References
- Ajello, M., Rau, A., Greiner, J., et al. 2008, *ApJ*, 673, 96
 Anders E. & Grevesse N., 1989, *Geochimica et Cosmochimica Acta* 53, 197
 Avni, Y. 1976, *ApJ*, 210, 642
 Bassani, L., Molina, M., Malizia, A., et al. 2006, *ApJ*, 636, L65
 Bassani, L., Malizia, A., Stephen, J. B., & for the INTEGRAL AGN survey team 2006, in proc. "6th INTEGRAL Workshop "The Obscured Universe"" (Moscow), ArXiv Astrophysics e-prints, arXiv:astro-ph/0610455
 Beckmann, V., Gehrels, N., Shrader, C. R., & Soldi, S. 2006, *ApJ*, 638, 642
 Bennett, C. L., Halpern, M., Hinshaw, G., et al. 2003, *ApJS*, 148, 1
 Bird, A. J., Malizia, A., Bazzano, A., et al. 2007, *ApJS*, 170, 175
 Bird, A. J., Barlow, E. J., Bassani, L., et al. 2006, *ApJ*, 636, 765
 Cappi, M., Panessa, F., Bassani, L., et al. 2006, *A&A*, 446, 459
 Cappi, M., Mihara, T., Matsuoka, M., et al. 1996, *ApJ*, 458, 149
 Comastri, A., Gilli, R., Vignali, C., et al. 2007, *Progress of Theoretical Physics Supplement*, 169, 274
 Gandhi, P., Fabian, A. C., Suebsuwong, T., et al. 2007, *MNRAS*, 382, 1005
 Dadina, M. 2008, ArXiv e-prints, 801, arXiv:0801.4338
 Deluit, S., & Courvoisier, T. J.-L. 2003, *A&A*, 399, 77
 De Rosa, A., Bassani, L., Ubertini, P., et al. 2008, ArXiv e-prints, 801, arXiv:0801.4675
 Elitzur, M., & Shlosman, I. 2006, *ApJ*, 648, L101
 Gallo, L. C., Fabian, A. C., Boller, T., & Pietsch, W. 2005, *MNRAS*, 363, 64
 George, I. M., & Fabian, A. C. 1991, *MNRAS*, 249, 352
 Gilli, R., Comastri, A., & Hasinger, G. 2007, *A&A*, 463, 79
 Goldwurm, A., David, P., Foschini, L., et al. 2003, *A&A*, 411, L223
 Gondek, D., Zdziarski, A. A., Johnson, W. N., et al. 1996, *MNRAS*, 282, 646
 Gondoin, P., Orr, A., Lumb, D., & Siddiqui, H. 2003, *A&A*, 397, 883
 Guainazzi, M., Matt, G., Molendi, S., et al. 1999, *A&A*, 341, L27
 Fabian, A. C., Miniutti, G., Iwasawa, K., & Ross, R. R. 2005, *MNRAS*, 361, 795
 Fabian, A. C., Miniutti, G., Gallo, L., et al. 2004, *MNRAS*, 353, 1071
 Feldmeier, J. J., Brandt, W. N., Elvis, M., et al. 1999, *ApJ*, 510, 167
 Haardt, F., & Maraschi, L. 1991, *ApJ*, 380, L51
 Kawaguchi, T., Shimura, T., & Mineshige, S. 2001, *ApJ*, 546, 966
 Krivonos, R., Vikhlinin, A., Churazov, E., et al. 2005, *ApJ*, 625, 89
 Lamer, G., Uttley, P., & McHardy, I. M. 2003, *MNRAS*, 342, L41
 Lebrun, F., Leray, J. P., Lavocat, P., et al. 2003, *A&A*, 411, L141
 Maiolino, R. 2001, *X-ray Astronomy: Stellar Endpoints, AGN, and the Diffuse X-ray Background*, 599, 199
 Malizia, A., Landi, R., Bassani, L., et al. 2007, *ApJ*, 668, 81
 Malizia, A., Bassani, L., Capalbi, M., et al. 2003a, *A&A*, 406, 105
 Malizia, A., Bassani, L., Stephen, J. B., et al. 2003b, *ApJ*, 589, L17
 Malzac, J., & Petrucci, P.-O. 2002, *MNRAS*, 336, 1209
 Malzac, J., Beloborodov, A. M., & Poutanen, J. 2001, *MNRAS*, 326, 417
 Malzac, J. 2001, *MNRAS*, 325, 1625
 Markwardt, C. B., Tueller, J., Skinner, G. K., et al. 2005, *ApJ*, 633, L77
 Masetti, N., Morelli, L., Palazzi, E., et al. 2006a, *A&A*, 459, 21
 Masetti, N., Pretorius, M. L., Palazzi, E., et al. 2006b, *A&A*, 449, 1139
 Masetti, N., Palazzi, E., Bassani, L., Malizia, A., & Stephen, J. B. 2004, *A&A*, 426, L41
 Mattson, B. J., Weaver, K. A., & Reynolds, C. S. 2007, *ApJ*, 664, 101
 McKernan, B., Yaqoob, T., & Reynolds, C. S. 2007, *MNRAS*, 379, 1359
 Merloni, A., Malzac, J., Fabian, A. C., & Ross, R. R. 2006, *MNRAS*, 370, 1699
 Miniutti, G., Fabian, A. C., Anabuki, N., et al. 2007, *PASJ*, 59, 315
 Miniutti, G., & Fabian, A. C. 2004, *MNRAS*, 349, 1435
 Molina, M., Malizia, A., Bassani, L., et al. 2006, *MNRAS*, 371, 821
 Nandra, K., O'Neill, P. M., George, I. M., & Reeves, J. N. 2007, *MNRAS*, 382, 194
 Nandra, K., & Pounds, K. A. 1994, *MNRAS*, 268, 405
 Perola, G. C., Matt, G., Cappi, M., et al. 2002, *A&A*, 389, 802
 Perola, G. C., Matt, G., Fiore, F., et al. 2000, *A&A*, 358, 117
 Petrucci, P. O., Ponti, G., Matt, G., et al. 2007, *A&A*, 470, 889
 Petrucci, P. O., Haardt, F., Maraschi, L., et al. 2001, *ApJ*, 556, 716
 Piconcelli, E., Sanchez-Portal, M., Guainazzi, M., et al. 2006, *A&A*, 453, 839
 Piconcelli, E., Jimenez-Bailón, E., Guainazzi, M., et al. 2005, *A&A*, 432, 15
 Piro, L. 1999, *Astronomische Nachrichten*, 320, 236
 Ponti, G., Miniutti, G., Cappi, M., et al. 2006, *MNRAS*, 368, 903
 Porquet, D., Reeves, J. N., Markowitz, A., et al. 2007, *A&A*, 466, 23
 Pounds, K. A., Reeves, J. N., Page, K. L., & O'Brien, P. T. 2004, *ApJ*, 605, 670
 Pounds, K., & Reeves, J. 2002, in proc. "New Visions of the X-ray Universe in the XMM-Newton and Chandra Era" (Noordwijk:ESA), ArXiv Astrophysics e-prints, arXiv:astro-ph/0201436
 Reeves, J. N., & Turner, M. J. L. 2000, *MNRAS*, 316, 234
 Risaliti, G., Maiolino, R., & Salvati, M. 1999, *ApJ*, 522, 157
 Sazonov, S., Revnivtsev, M., Krivonos, R., Churazov, E., & Sunyaev, R. 2007, *A&A*, 462, 57
 Sazonov, S. Y., Revnivtsev, M. G., Lutovinov, A. A., Sunyaev, R. A., & Grebenev, S. A. 2004, *A&A*, 421, L21
 Schurch, N. J., & Warwick, R. S. 2002, *MNRAS*, 334, 811
 Stephen, J. B., Bassani, L., Malizia, A., et al. 2006, *A&A*, 445, 869
 Tueller, J., Mushotzky, R. F., Barthelmy, S., et al. 2008, ArXiv e-prints, 711, arXiv:0711.4130
 Turner, T. J., Kraemer, S. B., George, I. M., Reeves, J. N., & Bottorff, M. C. 2005, *ApJ*, 618, 155
 Ubertini, P., Lebrun, F., Di Cocco, G., et al. 2003, *A&A*, 411, L131
 Vaughan, S., & Edelson, R. 2001, *ApJ*, 548, 694
 Winter, L. M., Mushotzky, R. F., Tueller, J., & Markwardt, C. 2008, *ApJ*, 674, 686
 Zdziarski, A. A., Poutanen, J., & Johnson, W. N. 2000, *ApJ*, 542, 703
 Zdziarski, A. A., Lubinski, P., & Smith, D. A. 1999, *MNRAS*, 303, L11
 Zdziarski, A. A., Johnson, W. N., Done, C., Smith, D., & McNaron-Brown, K. 1995, *ApJ*, 438, L63